Chemical Engineering Journal 359 (2019) 672–683

Contents lists available at ScienceDirect

Chemical Engineering Journal

journal homepage: www.elsevier.com/locate/cej

Halloysite nanotubes coated 3D printed PLA pattern for guiding human mesenchymal stem cells (hMSCs) orientation

Fan Wu, Jingqi Zheng, Zhixiong Li, Mingxian Liu*

Department of Materials Science and Engineering, Jinan University, Guangzhou 510632, PR China

HIGHLIGHTS

- Polydopamine was used to bond halloysite nanotubes on 3D printed PLA.
- HNTs coating can improve surface roughness and hydrophilicity of PLA pattern.
- PLA pattern with small strip width exhibits high ability to induce cell orientation.
- HNTs increase the adhesion and orientation of stem cells of PLA pattern.

GRAPHIC ABSTRACT

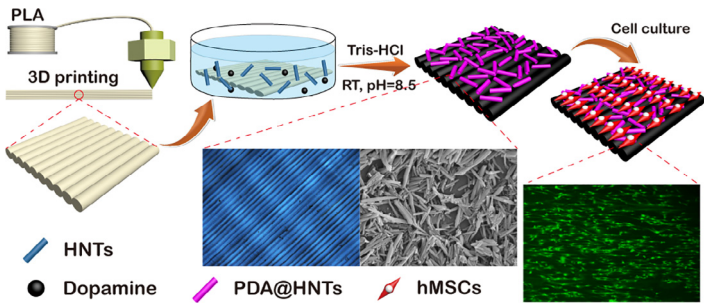

ARTICLE INFO

Keywords:
Halloysite nanotubes
Polylactic acid
Polydopamine
3D printing
Orientation

ABSTRACT

Three-dimensional (3D) printed polymer scaffolds can build engineered tissue constructs with complex and hierarchical structures, mechanical and biological heterogeneity. However, the interactions between the scaffolds and cells should be optimally designed for their practical application. In this work, 3D printed polylactic acid (PLA) pattern was functionalized by a polydopamine (PDA) interlayer to firmly bond the halloysite nanotubes (HNTs) on the surfaces of the PLA pattern for guiding cell orientation. A series of 3D printed PLA patterns with different stripe widths were characterized by scanning electron microscopy (SEM), polarized light microscopy (POM), 3D optical profiler and so on. The successful introduction of HNTs on PLA pattern was verified by field emission scanning electron microscopy (FE-SEM), X-ray photoelectron spectroscopy (XPS), water contact angle (WCA), Fourier transform infrared spectroscopy (FTIR), and thermogravimetric analyzer (TGA). The HNTs coating could effectively improve roughness and hydrophilicity of PLA pattern. In addition, *in vitro* human mesenchymal stem cells (hMSCs) culture experiments suggested that 3D printed PLA patterns with different strip widths exhibited different ability to induce cell orientation. The smaller the stripe width of the PLA pattern, the more suitable for cell orientation. When the layer height was set to 0.05 mm, the effect of inducing cell orientation was optimal. Meanwhile, the 3D printed PLA pattern with HNTs coating was more suitable for the adhesion and proliferation of cells. This works provides a general routine for improving the cell affinity of 3D printed PLA structure by the simple coating of nanoparticles, which shows the promising application in cell culture scaffolds, wound healing materials, and biosensors.

* Corresponding author.
E-mail address: liumx@jnu.edu.cn (M. Liu).

https://doi.org/10.1016/j.cej.2018.11.145
Received 28 August 2018; Received in revised form 15 October 2018; Accepted 18 November 2018
Available online 19 November 2018

1. Introduction

Cell orientation technology is a useful tool for biomedical research. Good cell orientation contributes to the study of basic cell biology, biomedical engineering such as cell-based biosensors, diagnostic equipment, cell-based devices for drug screening, and basic research on cell-material interactions [1,2]. Cell orientation depends on the interaction of the cells with the biological material, including both the surface properties and biological response of biological material. It has been reported that different surface patterns have been used for tailoring the interaction of biological materials with the biological environment [3,4]. For example, cell orientation can be achieved by patterning the material into micro/nano array structure. The main methods of constructing patterned surface include lithography [5], electrochemical etching [6], soft etching [7], self-assembly [8], electrospinning [9] and nanoimprinting [10]. However, these methods are complicated, and the process is expensive with the harsh experimental conditions.

Three-dimensional (3D) printing has received widespread attention in recent years, as 3D printing is capable of creating 3D geometries with precisely defined microstructures that result in superior material properties. It is a better choice to prepare the pattern of the micro/nano structure via the method of 3D printing. The current 3D printing technology mainly has fused deposition modeling (FDM), Polyjet, selective laser sintering (SLS), direct ink writing (DIW), and stereolithography (SLA), the digital light processing (DLP) [11]. Among them, FDM is the most common method in 3D printing technology, which manufactures 3D models by extruding thermoplastic materials. A notable advantage of FDM is that it can create objects fabricated from multiple material types, which enables more user control over device fabrication for experimental use [12]. Thermoplastics for 3D printing covered polylactic acid (PLA), polyglycolic acid (PGA), polycaprolactone (PCL), poly(lactic-co-glycolic acid (PLGA), etc. Specially, 3D printing PLA materials have been widely used in biomedical fields [13–15]. PLA has many advantages for 3D printing such as good thermal stability [16], proper processing temperature, good solvent resistance, biodegradability, biocompatibility [17], gloss, and transparency. However, there are still some drawbacks for using PLA as a biological material, such as hydrophobicity, smooth surface and cell adhesion difficulty, which limit the requirements of actual clinical use. Therefore, it is necessary to coat a biologically active coating to modify the PLA surface to obtain an improved performance of the biological material [18].

In recent years, as a natural one-dimensional (1D) nanomaterial with abundant resource, halloysite nanotubes (HNTs) have attracted widespread attention. HNTs have a chemical formula of $Al_2Si_2O_5(OH)_4{\cdot}nH_2O$, which is similar to kaolinite [19]. The inner diameter of the HNTs is in 10–20 nm and the length ranges from 200 to 1000 nm, which gives a high aspect ratio. HNTs have many advantages, such as large surface area, good biocompatibility, rich pore structure, sufficient surface hydroxyl groups, low cost, good mechanical properties [20]. Previous studies suggested that HNTs can be used as an additive in coatings to produce functional composites [21,22]. For example, HNTs have been coated on polyurethane foam from aqueous suspensions to create multilayered nanocomposite coatings. And the HNTs coating significantly reduces polyurethane flammability [23]. A highly oriented layer of HNTs on polyacrylonitrile porous membrane prepared via an evaporation-induced method allowed for the excellent dye rejection with high salt permeation, and thus these membranes were suitable for dye purification or concentration [24]. HNTs together with reduced graphene oxide (rGO) can be assembled on the surface of commercial cellulose acetate membrane, which exhibited the superior anti-fouling capacity and promising application in water purification and oil/water separation [25]. HNTs coatings can also capture tumor cells from cancer patient blood with high capture efficiency, and the captured cells showed more spreading morphology [26]. Very recently, HNTs loaded with dyes or drug were self-assembled on hair allowing for coloring or medical treatment. This facile process can result in a ~3 μm thick uniform hair surface coating [27]. The toxicity research of HNTs and their composites showed that HNTs were safe for cells and animals within a certain concentration [28]. In human cell cultures, HNTs-quantum dots hybrid could be internalized by living cells and demonstrated intense and stable fluorescence combined with pronounced nanotube light scattering [29]. Biopolymer-HNTs composites were safe for cell culture up to 0.5 mg/mL [30]. HNTs were also considered to be a biosafe material such as plants, microalgae chlorella, ciliate native paramecium, Escherichia coli, Zebrafish, and the like [31]. In addition, HNTs oil/water emulsion was shown to be capable of efficient interfacial catalytic reactions [32].

In our previous work, the patterned HNTs surfaces exhibit a high contact guiding ability for cell growth. For example, the concentric ring-like HNTs pattern prepared via evaporation-induced self-assembly can guide the growth and orientation of C2C12 myoblast cells perpendicular to the rings [24]. In this study, we have prepared a HNTs coated 3D printed PLA pattern for guiding cell orientation. The HNTs coating was fixed on the surface of the 3D printed PLA pattern by polydopamine (PDA). PDA modification does not require complex chemical reactions and is suitable for any type of material, it can achieve adhesion of the HNTs coating to the surface of the PLA pattern [33]. Although different machines can control the stripe and roughness of the PLA, they are usually complex and very expensive. The surface treatment technology of the common 3D printed PLA pattern via soaking of HNTs dispersion is simple, divers, and low cost. The morphology, thermal stability, surface composition, and hydrophilicity of the untreated and HNTs coated PLA pattern were evaluated in details. The cytocompatibility of the coated PLA pattern was comprehensively studied in terms of the adhesion, proliferation and orientation behavior of the human mesenchymal stem cells (hMSCs). The PDA decorated HNTs coating not only improves the roughness of the material but also significantly enhances the cell adhesion and proliferation of the material. The study laid the foundation for the application of nanotubes coated PLA scaffold in the regeneration of nerves, tendons, regeneration of skin, vascular grafts, and tissue engineering.

2. Experimental

2.1. Materials and reagents

HNTs were purchased from Guangzhou Runwo Materials Technology Ltd., China. PLA granules were purchased from UNIC Technology Ltd., China. Tris (hydroxymethyl) aminomethane (Tris) and dopamine hydrochloride were bought from Aladdin Bio-Chemical Technology Ltd., China. Other chemicals used in this study were of analytical grade and used as received. Ultrapure water was purified by deionization and filtration with a Millipore purification apparatus (resistivity > 18.2 MΩ·cm).

2.2. Preparation of PLA filament for 3D printing and 3D printed PLA pattern

Firstly, the PLA granules were dried in an oven at 60 °C for 3 h, then extruded in a single screw extruder (HTES-25, Guangzhou Hartek Machinery Ltd., China) with a die temperature of 170 °C and wire diameter of 3 mm. PLA patterning material is prepared by using a 3D printer (WBFDM211515, Winbo Smart Tech Ltd., China). The Autodesk 3ds Max 2017 computer software modeling program was used to design the 3D print files and transferred to a 3D printable format using the Repetier-Host software. The resulting generated STL file was used to dictate the construct dimensions to the printer through Repetier-Host. Extrusion temperature was set as 215 °C, nozzle diameter was 0.4 mm and layer height was 0.05, 0.1, 0.2, and 0.3 mm, respectively. The travelling speed was 150 mm/s.

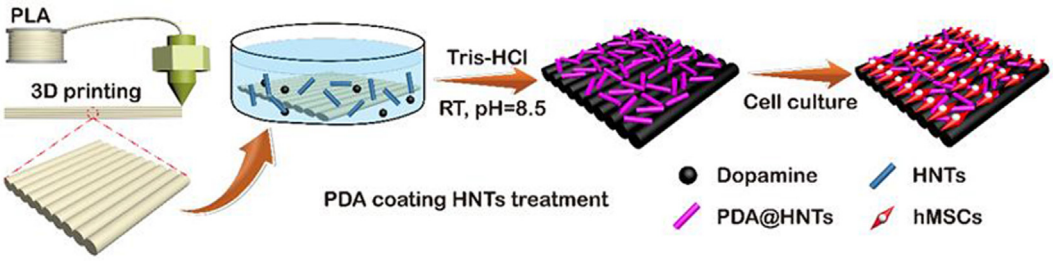

Fig. 1. Schematic diagram of the preparation of HNTs coated PLA pattern for guiding cell orientation.

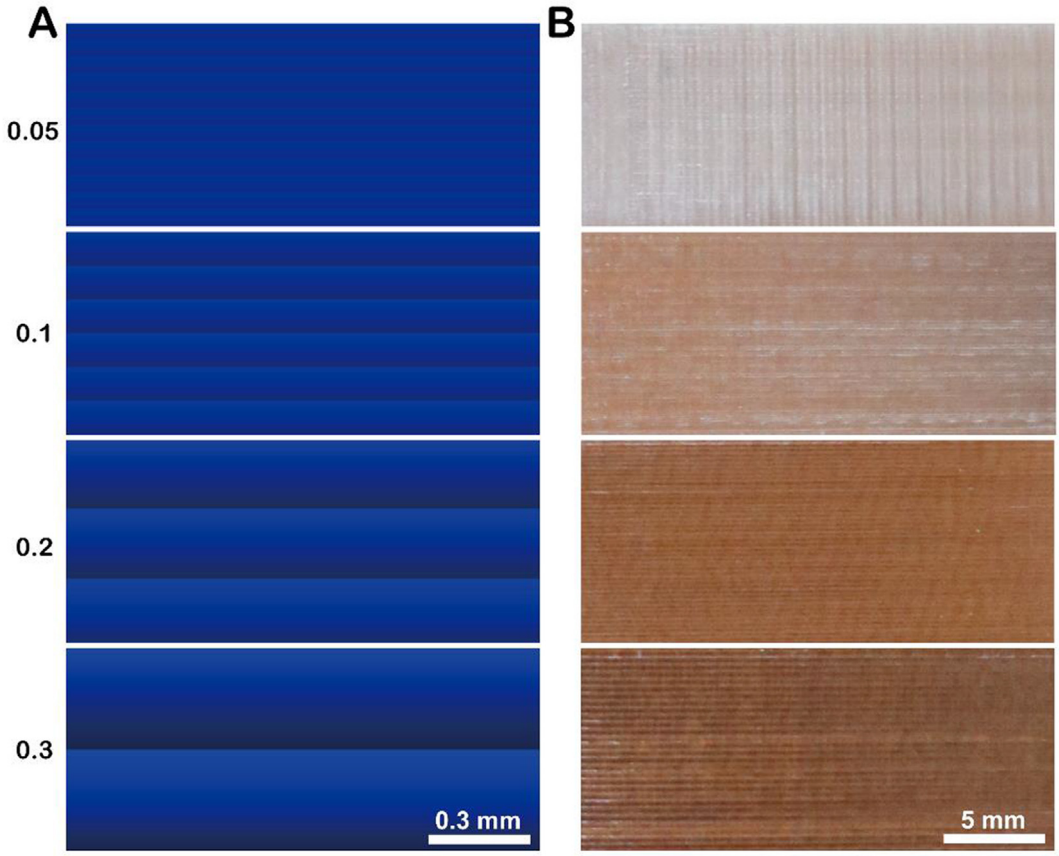

Fig. 2. The images of the STL files from the slicing software (A) and the photographic images of the PLA pattern surfaces in different stripe widths (B).

2.3. Preparation of HNTs coated 3D printed PLA pattern

The process of preparing HNTs coated 3D printed PLA pattern is shown in Fig. 1. Firstly, before the coating process, ultrapure water was used to clean the surface of the PLA pattern and the pattern was then dried at room temperature. Then, 4.0 g of HNTs was dispersed by ultrasonication treatment in a 100 mL Tris-HCl (10 mM, pH 8.5) buffer solution for 30 min. Afterwards, dopamine solution (0.2 g of dopamine hydrochloride dissolved in 10 mM Tris buffer, pH 8.5, volume: 100 mL) was added to the HNTs dispersion solution, and then the prepared PLA pattern was quickly added. The 3D printed PLA pattern within the HNTs solution was shaken at 300 r/min for 24 h in a shaker, and finally the 3D printed PLA pattern was washed several times with a large amount of ultrapure water to remove excess PDA. Vacuum dried was used to obtain HNTs coated 3D printed PLA pattern. The PDA decorated HNTs was denoted as PDA@HNTs.

2.4. Characterizations of the untreated and treated 3D printed PLA pattern

2.4.1. Scanning electron microscope (SEM)

Before SEM observation, the samples were sputter-coated with gold films with a thickness of 5 nm. The shape of the stripe of the 3D printed PLA pattern was detected by tabletop SEM (TM3030, Hitachi Ltd., Japan) at EDX.

2.4.2. Field emission scanning electron microscope (FE-SEM)

Before FE-SEM observation, the samples were sputter-coated with gold films with a thickness of 5 nm. The surface morphology of the HNTs coated 3D printed PLA pattern was observed by a FE-SEM (ULTRA55, Carl Zeiss Jena Ltd., Germany) at 5 kV.

2.4.3. X-ray photoelectron spectrum (XPS)

X-ray photoelectron spectroscopy was analyzed by X-ray photoelectron spectroscopy instrument (ESCALAB250Xi, Thermo Fisher Scientific Ltd., USA). The atoms of N, C, O, Al and Si were detected.

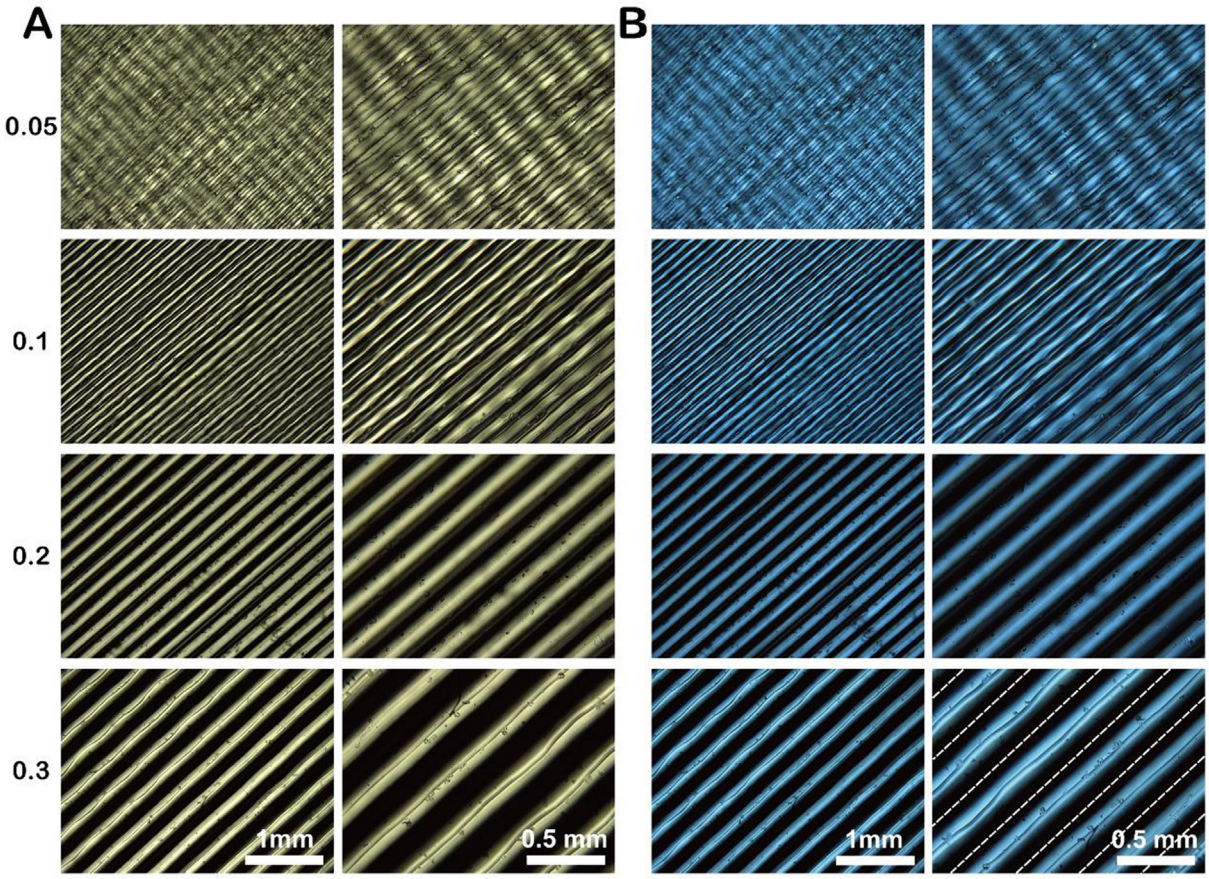

Fig. 3. Polarized light microscope images of the PLA pattern surfaces in different magnifications and different stripe widths: White light (A); Polarized light (B) (region between the two dots lines represents a single stripe).

2.4.4. Polarized optical micrographs (POM)

The untreated and HNTs coated 3D printed PLA pattern was placed on a glass sheet, and then the photographs were taken by using the polarized optical microscope (BX51, Olympus Corporation, Japan).

2.4.5. 3D morphology

The surface morphology and roughness of the 3D printed PLA pattern were detected by a 3D optical profilometer (UP-DUAL MODE, Rtec Engineering Ltd., USA) with magnification of 200 X. The 3D profile of the coating surface was inspected with a 3D optical profiler with a test area of 1 mm × 1 mm (CF mode). The line profiles are obtained by analyzing the 3D topography by Gwyddion analysis software.

2.4.6. Water contact angle (WCA)

The surface hydrophilicity of the 3D printed PLA pattern was determined using a drop-shape analyzer (DSA100, Kruss Ltd., Germany) at room temperature. The contact angle was measured just after the liquid deposition onto the substrate. The liquid droplet volume was 5.0 ± 0.5 μL. Five measurements at least were carried out on each sample.

2.4.7. Transmission electron microscopy (TEM)

The morphology of HNTs and PDA@HNTs was observed by TEM (JEM-2100F, JEOL Ltd., Japan) under an accelerating voltage of 100 kV, The sample was ultrasonically dispersed in ultrapure water and dropped on the copper network before observation.

2.4.8. Fourier transform infrared spectroscopy (FTIR)

Surface functional groups were determined by FTIR and tested using attenuated total reflection (ATR) model in a Thermo FTIR (Nicolet iS50, Thermo Fisher Scientific Ltd., USA). The spectra were recorded from 4000 to 500 cm^{-1}.

2.4.9. X-ray diffraction (XRD)

XRD patterns were determined by XRD (Miniflex600, Rigaku Corporation, Japan) at an accelerating voltage of 40 kV and the current of 40 mA.

2.4.10. Thermo gravimetric analyzer (TGA)

TGA curves were tested using the TGA (TGA2, METTLER TOLEDO, Ltd., Switzerland) under a nitrogen atmosphere from 50 °C to 600 °C at a heating rate of 10 °C/min.

2.5. Cell culture

Mouse embryo osteoblast precursor (MC3T3-E1) cells were purchased from the laboratory animal center of Sun Yat-Sen University, China. And hMSCs were purchased from Cyagen Biosciences Inc, USA. MC3T3-E1 cells were cultured in Dulbecco's modified Eagle's medium (DMEM, Thermo Fisher Scientific Ltd., USA), with 10% (v/v) fetal bovine serum (FBS, Thermo Fisher Scientific Ltd., USA) and 1% (v/v) penicillin-streptomycin solution (Jiangsu KeyGEN BioTECH Ltd., China) at 37 °C, 5% carbon dioxide (CO_2). hMSCs were cultured in Basal medium (DMEM, Cyagen Biosciences Inc. USA), with 10% (v/v) fetal bovine serum (FBS, Cyagen Biosciences Inc. USA) and 1% (v/v) penicillin-streptomycin solution (Cyagen Biosciences Inc. USA) at 37 °C, 5% carbon dioxide (CO_2). The cells were grown to 80% confluences before passaging with trypsin/ethylenediaminetetraacetic acid (EDTA, Jiangsu KeyGEN BioTECH Ltd., China) incubation for 1 min. Prior to the cell experiment, the 3D printed PLA pattern was cut into the appropriate

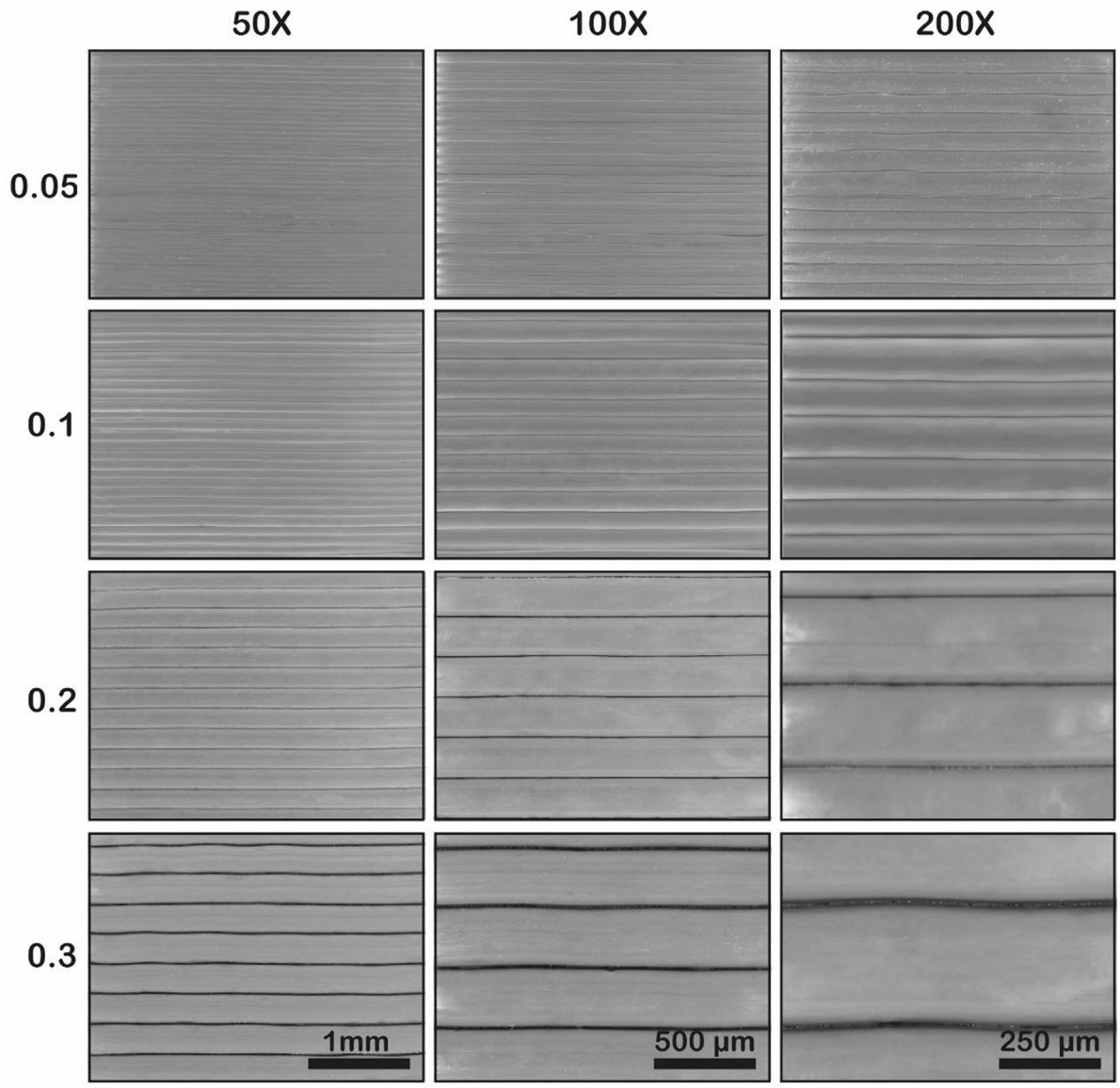

Fig. 4. SEM images of the PLA pattern surfaces in different magnifications and different stripe widths.

size and placed in a cell culture plate, sterilized by adding 75% (v/v) alcohol overnight and ultraviolet light for 1 h. Then the cells were immersed in the cell culture medium for 2 h and washed twice with PBS. The cell culture medium was changed every two days.

2.6. Cell counting kit-8 (CCK-8) assays

Cell proliferation was evaluated using CCK-8 assay (BestBio biology Ltd., China). Cells were seeded onto the 3D printed PLA pattern ($3 \times 3 \times 0.3\,mm^3$) placed in 96-well cell culture plates (Wuxi NEST Biotechnology Ltd., China) at a seeding density of 1×10^4 cells per well, and cultured as mentioned above for different days. The cells were taken out from the medium and placed in new 96-well cell culture plates. Then, the PLA patterns were washed twice with 37 °C pre-sterilized Phosphate Buffered Saline (PBS, Thermo Fisher Scientific Ltd., USA) buffer solution (pH 7.4) and 100 mL fresh medium was added. After that, 10 μL CCK-8 reagents were added into each well and incubated at 37 °C for 4 h. After 4 h, put the above mixed solution into a new 96-well cell culture plate. The absorbance of the mixed solution was measured at 450 nm by means of enzyme-linked immunosorbent assay plate reader (MK3, Thermo Fisher Scientific Ltd., USA). Five measurements at least were carried out on each sample.

2.7. Cell morphology on 3D printed PLA pattern

Cells were seeded onto the 3D printed PLA pattern ($10 \times 10 \times 0.3\,mm^3$) placed in 24-well cell culture plates (Wuxi NEST Biotechnology Ltd., China) at a seeding density of 2×10^4 cells per wells and cultured as mentioned above for different days. Then, the culture medium in the well plate was aspirated and the cells were washed twice with 37 °C pre-sterilized PBS buffer solution (pH 7.4). Cell fixation was performed using 4% paraformaldehyde (PFA, Biosharp Ltd., China) at room temperature for 10 min. After that, permeabilized with 0.5% Triton X-100 (Biosharp Ltd., China) solution for 5 min. 200 μL of the prepared fluorescein isothiocyanate (FITC, Solarbio Technology Ltd., China) working solution or rhodamine (TRITC) phalloidin (Solarbio Technology Ltd., China) and 4′,6-diamidino-2-phenylindole (DAPI, Solarbio Technology Ltd., China) were added and incubated in the dark for 30 min at room temperature. Finally, the cells on the surface of the 3D printed PLA pattern were observed under a

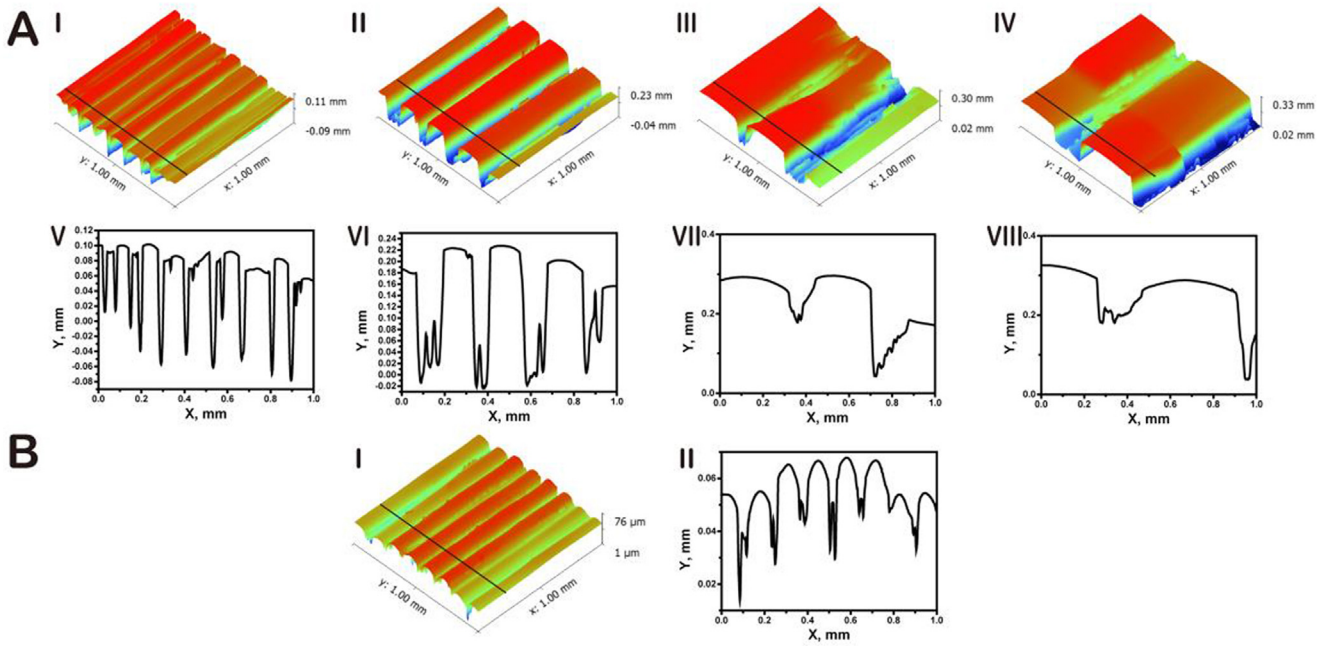

Fig. 5. 3D topography and roughness curve of the 3D printed PLA pattern surfaces in different stripe widths. Untreated PLA pattern (A): 0.05 mm (I and V), 0.1 mm (II and VI), 0.2 mm (III and VII), 0.3 mm (IV and VIII); HNTs coated PLA pattern (B): 0.05 mm (I and II). (straight black lines in the images represent corresponding line profiles positions).

fluorescence microscope (XDY-2, Guangzhou Liss Optical Instrument Ltd., China). We quantitatively counted the cell orientation alignment of hMSCs by Image J software and measured the average orientation angle of the cells, and 50 cells were counted for each sample.

3. Results and discussion

3.1. Structure of the 3D printed PLA pattern

PLA pattern is modeled by 3D modeling software to generate STL files and prepared by a universal 3D printer. Fig. 2B shows the digital photographs of PLA patterns of different stripe widths prepared by 3D printing. Similar to the STL file diagram of Fig. 2A, which forms regular parallel stripes in the 3D printing direction. As the stripe width of the 3D printed PLA pattern increases, the transparency of the PLA patterning structure increases. This can be understood by that smaller stripe width leads to denser array of the materials, which can affect the light transmission. It also can be seen whatever the width of the stripes is, the 3D printed PLA structure is uniform with relatively smooth surfaces.

The structure of 3D printed PLA pattern was then characterized by POM, SEM and 3D optical profile. Fig. 3 shows the microscope images 3D printed PLA pattern of different stripe widths under white light and polarized light. When the single PLA stripe is observed under polarized light, it can be seen that the central region is bright and the edge of the stripe is dark (Fig. S1A). This can be explained by that PLA is subjected to the shearing force during the 3D printing extrusion process, which results in the alignment of the molecular chains in the central region. From the images in Fig. 3B, parallel stripes with bright and dark are formed in all the samples, and the region between the two dots lines represent a single stripe. The width of the stripe for the four samples is determined as 0.468 ± 0.011, 0.102 ± 0.012, 0.202 ± 0.008, 0.291 ± 0.004 mm, respectively. When rotating the PLA pattern from 0° to 360°, the appearance of the pattern can transfer from dark to bright. The PLA pattern is totally bright when the stripes are in the 45° and 135° directions under the polarized light (Fig. S1B). This is attributed to the crystallization state of PLA stripes formed during the 3D printing. It can be seen that the strip width increases as the layer height increases. So, it is convenient to obtain PLA regular pattern with different stripe widths by adjusting the 3D printing parameter. The microstructure of the 3D printed PLA pattern was further observed by SEM (Fig. 4). Consistent with previous observation, when the layer height becomes larger, the width of the stripe of the PLA pattern increases and the gap between adjacent stripes is also larger. The width of the stripe for the four sample is also determined as 0.050 ± 0.004, 0.970 ± 0.08, 0.200 ± 0.004, 0.278 ± 0.002 mm, respectively, which is very close to the parameter of layer height. All the surfaces of the PLA pattern are smooth and clean, so these surfaces may not support the cell growth well since the cells relatively easily adhered on rough surfaces.

The 3D printing PLA pattern with different stripe widths is characterized by a 3D optical profilometer (Fig. 5). It also can be seen that the surface of PLA pattern with different stripe widths is smooth. The stripe width of the 3D printed PLA pattern is correlated with the layer height. The width and height of the five PLA pattern can be calculated by the roughness curve. The width of the stripe in 0.05, 0.1, 0.2, 0.3 and 0.05-HNTs sample is 0.063 ± 0.036 mm, 0.144 ± 0.019 mm, 0.304 ± 0.084 mm, 0.464 ± 0.063 mm, and 0.086 ± 0.010 mm, respectively. It can be seen the determined size of the stripe is much higher than that of the layer height. The 3D optical profilometer is determined according to the optical principle, which may bring some error. However, after coating of HNTs, the surface is much rougher than that untreated surface (Fig. 5I). Also, the height of the HNTs-treated PLA stripe is much higher than that pure PLA stripe.

3.2. Characterization of HNTs coated PLA pattern

To increase surface roughness and cell affinity of the PLA pattern, a layer of HNTs is coated with the aid of dopamine. Dopamine can be easily polymerized under weak base condition at room temperature on many substrates, and polydopamine (PDA) is considered as a bioadhesive [34]. PDA has also been used to treat HNTs surface to obtain surface modified nanotubes [35–38]. In the present work, the color of dopamine and halloysite mixed solution in which the PLA pattern is immersed changed from white to gray and finally to black, suggesting the polymerization of dopamine on PLA pattern. In this process, the

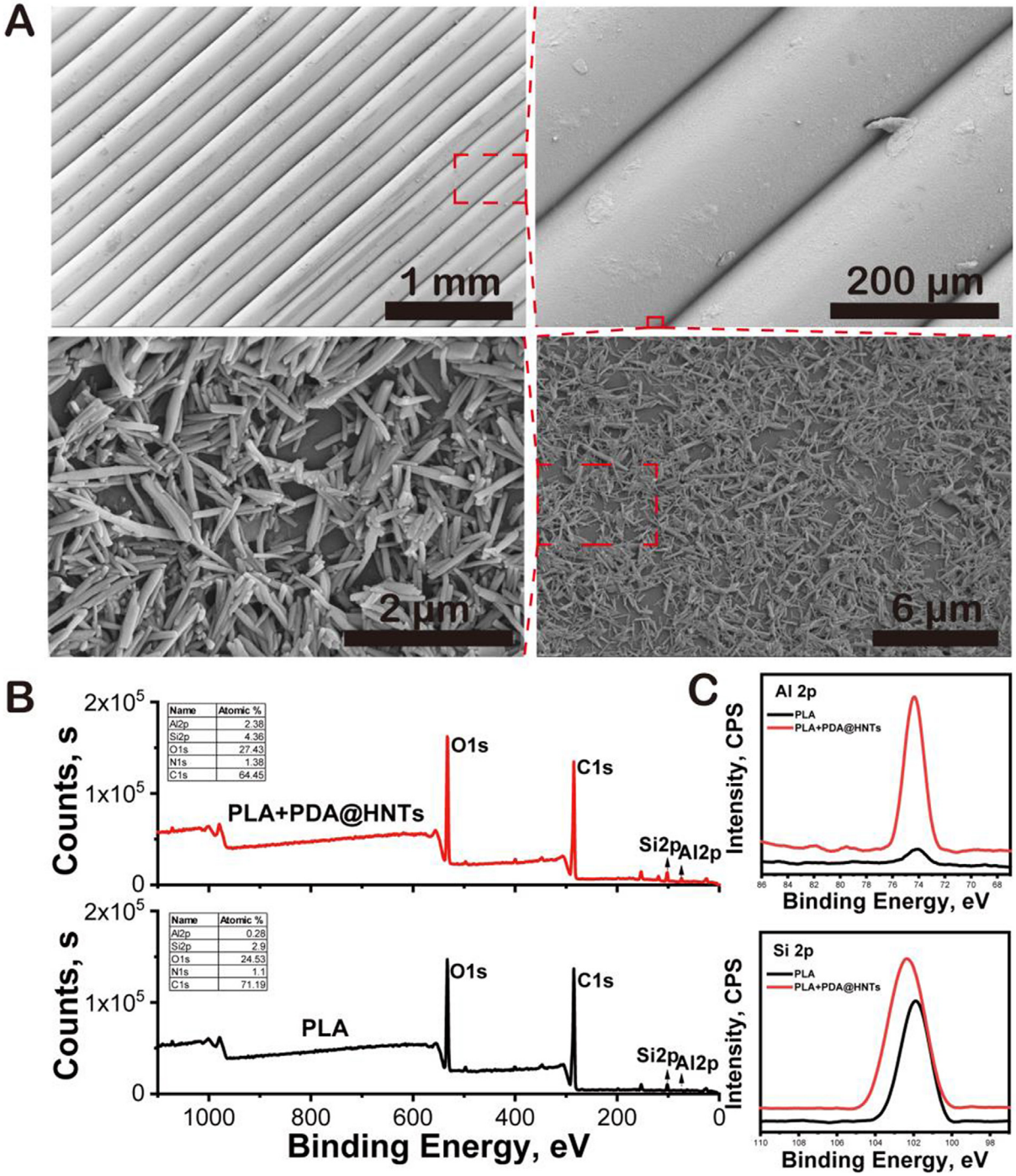

Fig. 6. FE-SEM images of HNTs coated PLA pattern surfaces with different magnification (A). XPS spectra of PLA pattern and HNTs coated PLA pattern (B and C).

HNTs layer has adhered on the PLA pattern surfaces. TEM image of HNTs before and after PDA treatment, the diameter of the HNTs is significantly increased (Fig. S2). This is because dopamine self-polymerizes under alkaline conditions, producing a black layer of PDA [39]. The polarized light microscope was further used to characterize the HNTs coating modified PLA pattern. As shown in Fig. S3, after the modification of the HNTs coating, the image of the PLA pattern became darker than that of Fig. 3. But the crystallization state of PLA does not change significantly, which suggests that the surface treatment only takes place on the outer surfaces of PLA pattern and it does not change the bulk properties of PLA. Therefore, the HNTs coating can be successfully coated on the 3D printed PLA structure without harming the basic properties of PLA.

The surface topography of the HNTs coated 3D printed PLA pattern was characterized by FE-SEM (Fig. 6A). It is apparent that the HNTs are uniformly distributed with the arbitrary arrangement on the surface of the PLA pattern because of no shear force applied, and the striped structure of the PLA pattern is not destroyed. This indicates that PDA@HNTs are easily adsorbed on the PLA pattern, and HNTs are not easily detached from the PLA pattern in practical applications. The treated PLA surfaces undergo washing and sterilization process before cell culture, however, the PDA@HNTs layers do not easily fall off the surface of PLA pattern. Actually, the use of mussel-inspired binder dopamine as a site-specific anchor on HNTs for design of functional coating

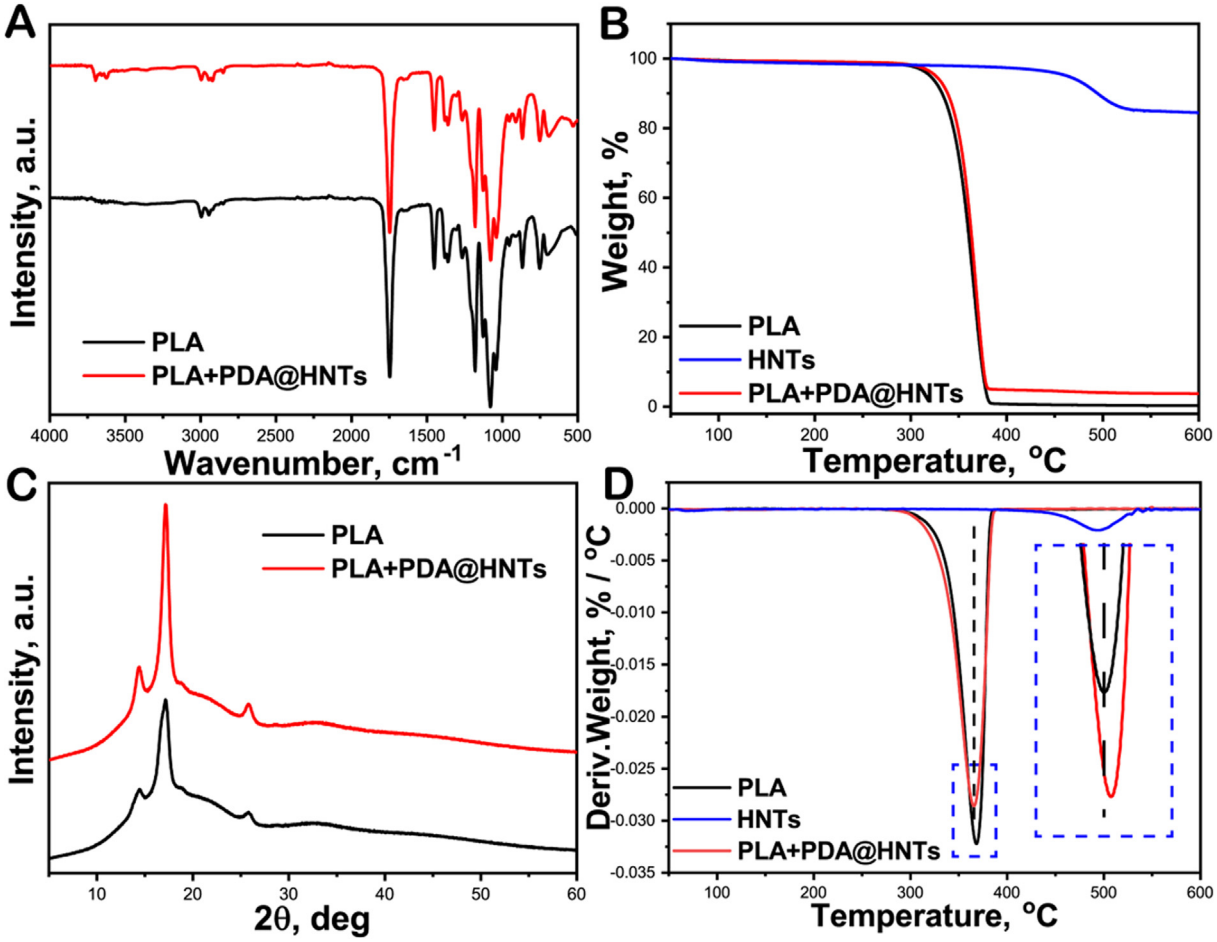

Fig. 7. FTIR spectra (A), TG curves (B), XRD patterns (C) and DTG curves (D) of PLA pattern and HNTs coated PLA pattern.

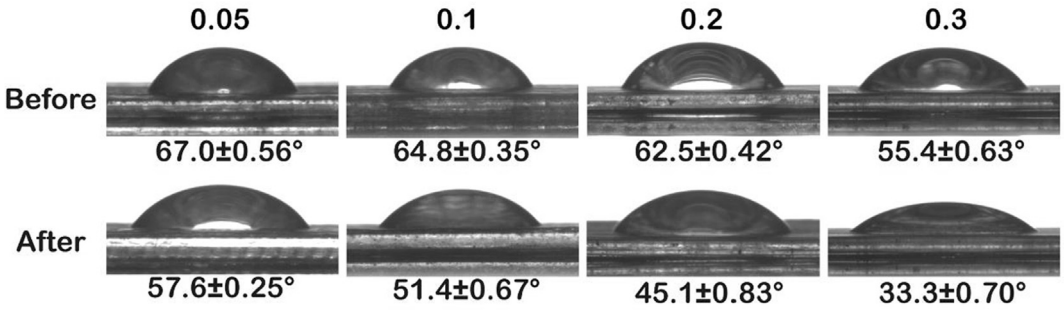

Fig. 8. Contact angle images of the PLA pattern surfaces with different stripe widths before and after HNTs coating.

on different polymers has been widely reported, which is an efficient and feasible method to endow biological functionality on HNTs because of no complex linkers and free of organic solvents involved [38–40]. However, if no HNTs are incorporated, the self-polymerized PDA on PLA surface is located between the neighbored PLA stripes (Fig. S4). The polymerization of dopamine on PLA pattern surfaces is uniform. However, PDA agglomerate between neighbored strips is more difficult to wash off, so the PDA is located in the gap of PLA strips. Due to interactions between PDA and HNTs, and the HNTs coating is uniformly and firmly bonded to the surface of the PLA pattern. When dopamine is oxidized and polymerized to form polydopamine, a crosslinked molecular structure is formed. Although the polymerization occurs quickly in alkaline condition and in the presence of oxygen, the polymerization product is complicated. The molecular weight (or polymerization degree) of the crosslinked PDA is hardly to measured [41]. To further show the successful introduction of HNTs on PLA surfaces, XPS scanning for the untreated and treated surface was conducted (Figs. 6B and 7C). A significant difference between the elemental compositions of the 3D printed PLA pattern before and after HNTs coating is found. The main chemical composition of HNTs is oxygen (53.72%), aluminum (11.46%), and silicon (13.23%) [42]. And the characterized element of PDA is nitrogen. Increase in oxygen and nitrogen content and decrease in carbon content after treatment suggest PDA@HNTs are coated on PLA surfaces. HNTs coating results in the content of aluminum, silicon, nitrogen, oxygen increases from 0.28% to 2.38%, from 2.9% to 4.36%, from 1.1% to 1.38%, from 24.53% to 27.43%, respectively. In contrast, content of carbon decreases from 71.19% to 64.45% after treatment. The nitrogen element of pure PLA may arise from the tiny contaminant on the surfaces (dander, bacteria, microorganisms, etc.). As shown in Fig. 6C, the high-resolution spectra of XPS Al2p and Si2p also indicates

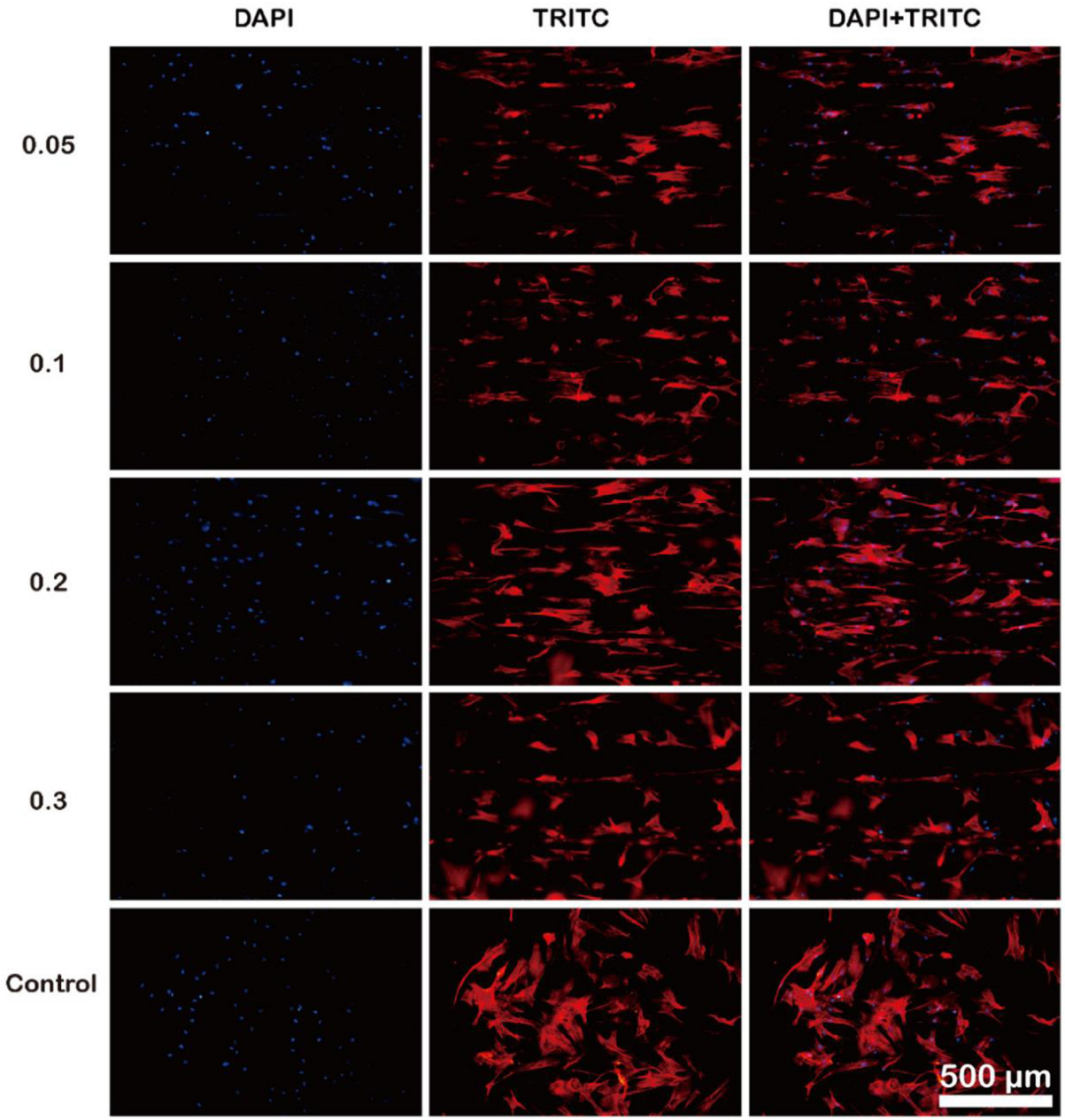

Fig. 9. Fluorescence micrographs of hMSCs stained with DAPI and TRITC seeding on HNTs coated 3D printed PLA pattern surfaces in different stripe widths.

the adhesion of HNTs coating on the 3D printed PLA pattern, and the intensity of peaks of Al2p and Si2p significantly increases. The surface of the 3D printed PLA pattern is contaminated by dust in the air, thus the highly resolution spectrum of the 3D printed PLA pattern also has a Si2p photoelectron peak. Furthermore, the photoelectron peak of Si2p shifts in the direction of low binding energy compared to the 3D printed PLA pattern without the HNTs coating modified, which is attributed to the different chemical state of the contaminated silicon and silicone in HNTs.

In addition, the HNTs coated PLA pattern was further characterized by FTIR, TGA, and XRD. The peaks of HNTs (3692 and 3620 cm^{-1}) appear in the FTIR spectrum (Fig. 7A), which are attributed to the stretching vibration of the hydroxyl groups inside and outside the HNTs. There is no peak of PDA, which is attributed to that the amount of dopamine hydrochloride added is relatively small (0.2 wt%). The stronger absorption band of C═O group of PLA was shifted from 1746.0 cm^{-1} to 1746.5 cm^{-1} in the HNTs coating PLA pattern, which may be due to interfacial interactions between PDA@HNTs and PLA. The IR absorption band of C═O group of PLA was shifted from 1746.0 cm^{-1} to 1746.5 cm^{-1} in the coated PLA pattern (Fig. 7A), which may be due to interfacial interactions between the PDA@HNTs and PLA. TGA analysis can analyze the change in the weight of the PLA pattern during thermal decomposition (Fig. 7B and D). Pure PLA is almost completely decomposed in the temperature range of 300–400 °C, and the residue at 600 °C is 0.35%. Raw HNTs show 16.9% weight loss from 50 °C to 600 °C, which is mainly attributed to the loss of adsorbed water and hydroxyl dehydration. In contrast, when PDA@HNTs are coated on PLA pattern, the remaining weight of the composite at 600 °C is 3.78%. The amount of PDA@HNTs coated on PLA is 3.43% calculated from the TGA results. After the introduction of HNTs coating, the thermal stability of the PLA pattern is slightly improved. The maximum decomposition temperature (T_{max}) of PLA increases from 364.9 °C to 367.2 °C. These results confirm that HNTs coating is covered on the surfaces of the PLA pattern. The crystal structure of the PLA pattern

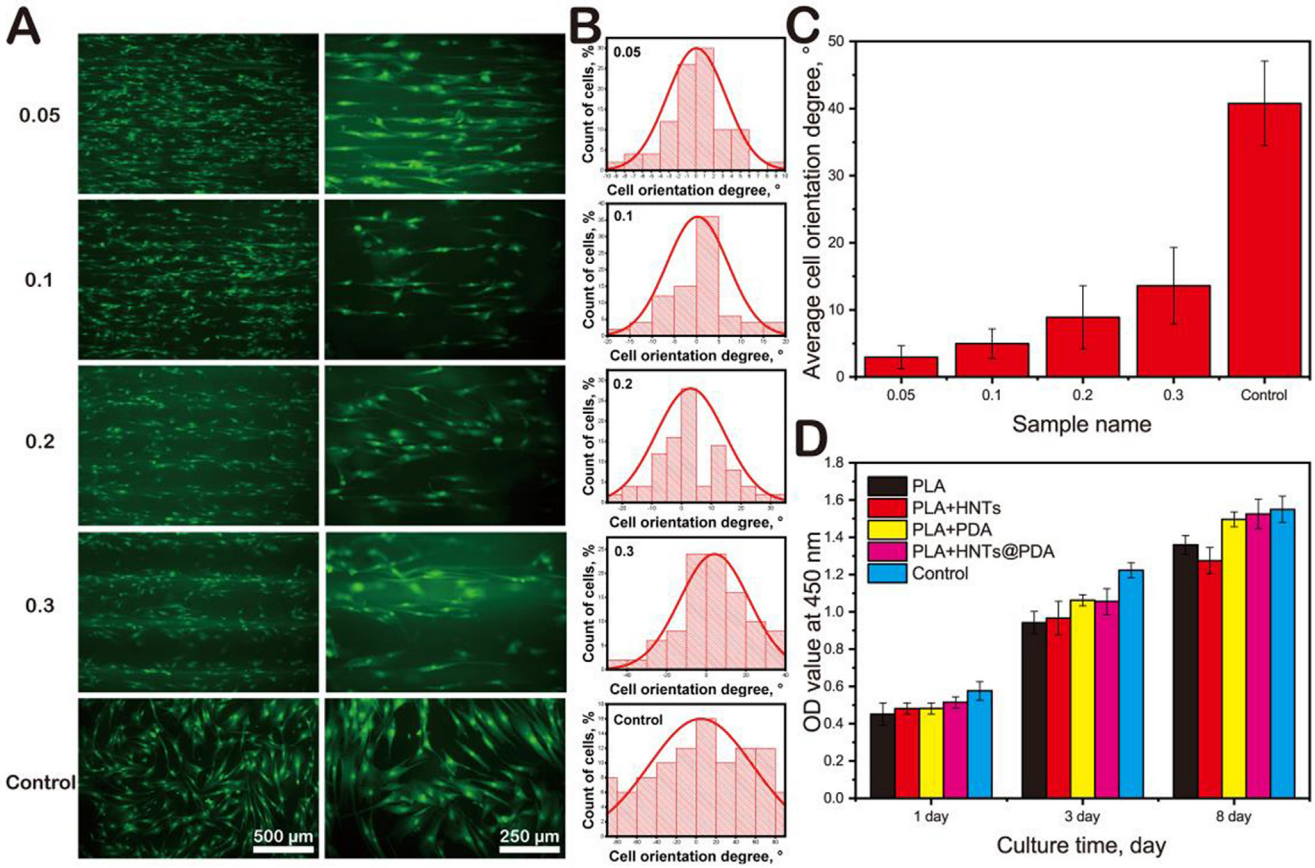

Fig. 10. Fluorescence micrographs of hMSCs stained with FITC seeding on HNTs coated 3D printed PLA pattern surfaces in different stripe widths (A). Distribution of orientation angles and average orientation angles for cells on PLA pattern surfaces in different stripe widths (B and C). The OD value of the hMSCs culturing on different modified 3D printed PLA patterns for 1,3, and 8 days (D).

before and after HNTs modification was characterized by XRD (Fig. 7C). The addition of the HNTs coating does not change the crystal structure of the PLA, and no new diffraction peak appears. This is also attributed to the low content of HNTs and the PDA is also amorphous [43].

The surface water contact angle reflects the hydrophilicity, which will affect protein adsorption and subsequent cell adhesion to PLA pattern [44]. Since PLA is a hydrophobic material, according to the literature, the fiber membrane produced by PLA electrospinning has a WCA of up to 149.5°, which is detrimental to protein adsorption and cell adhesion [45]. The influence of HNTs coating modification on the WCA of the 3D printed PLA pattern is shown in Fig. 8. Whether there is or not HNTs coating on 3D printed PLA pattern, the contact angles decrease as the stripe width of the PLA pattern increases. This is because the smaller the stripe width, the rougher the surface. The rougher the surface will improve the hydrophobicity of the material [46]. The HNTs coating can reduce the water contact angle of the PLA pattern surfaces and improve the hydrophilicity of the PLA pattern. The water contact angle of the surface of the 3D printed PLA pattern modified by the HNTs coating is as low as 33.3 ± 0.70°. Furthermore, the silanol groups on the surface of the HNTs and the phenolic hydroxyl groups on the surface of the PDA are more hydrophilic than the typical hydrophobic groups (alkyl and ester groups) on the surface of the PLA. After modification with the HNTs coating, the roughness is increased, resulting in an increase in the hydrophobicity of the material. However, this hydrophobicity is mainly controlled by the chemical groups rather than the slightly increased nanoroughness by HNTs. Therefore, the HNTs coating modified 3D printed PLA pattern has a smaller WCA and improved hydrophilicity than the unmodified PLA pattern.

3.3. *In vitro* evaluation of HNTs coated 3D printed PLA pattern

Cells grow in the direction of the groove, or anisotropic morphology induces cells to align and migrate along anisotropic directions. This phenomenon is recognized as “contact guidance” [47]. The orientation of cells produced by contact guidance is significant for the construction of cell-based biosensors, functional neural chips, large cell arrays, and wound healing [48–50]. As shown in Fig. S5, MC3T3-E1 cells were seeded in the prepared 3D printed PLA pattern for 2 days, and the cells can adhere to all surface 3D printed PLA patterns. Compared with the control group of the blank culture plate, MC3T3-E1 cells can be arranged in the stripe direction on all 3D printed PLA patterns. This indicates that the 3D printed PLA pattern has good biocompatibility and can guide cell orientation. From the result of the CCK-8 assay, the PDA@HNTs coated PLA pattern is less cytotoxic and has a larger cell diffusion area than the PLA pattern only coated with HNTs (without PDA). Therefore, the modification of HNTs coating by PDA can significantly improve the viability of MC3T3-E1 cells to adhere to PLA patterns (Fig. S5F). The PDA firmly fixes HNTs on the surface of the PLA pattern, which reduces the shedding of HNTs from the materials. HNTs may cause damage to cells due to their sharp edges of the tubes. So, incorporation of PDA increases the binding ability of HNTs on PLA pattern, which further increases the cell affinity [39,51]. Bioinspired PDA has served as a universal coating to nanoparticles for various biomedical applications. For example, *in vitro* study had shown that PDA-coated gold nanoparticles have low cytotoxicity and PDA coating was stable within cells of the liver and spleen for at least six weeks [52]. As shown in Fig. S6, fluorescence microscopy images of MC3T3-E1 cells after 5 days incubation show that different stripe widths have different ability to guide cell orientation. The smaller the stripe width, the

smaller the cell spreading area. The PLA pattern samples with 0.2 mm and 0.3 mm stripe width have substantially no cell orientation, but the sample with 0.05 mm stripe width has a better orientation than the sample with 0.1 mm width. This is because that cells can distinguish and adjust their shape according to the microstructure of the substrate material.

hMSCs were further seeded in the prepared 3D printed PLA pattern, and the cytotoxicity and morphology results are shown in Figs. 9 and 10A. After 5 days of incubation, hMSCs could be arranged in the stripe direction on all 3D printed PLA patterns of different stripe widths in comparison with the control group (blank culture plate). The different alignment ability between MC3T3-E1 cells and hMSCs arises the different cell sizes and characters. hMSCs are bigger than MC3T3-E1 cells, and the hMSCs possess a multipotent ability which usually are used to introduce tissue regeneration [53,54]. For the “contact guidance” effect, there were “critical dimensions” and “ the optimum size” [55]. When the pattern size is comparable with the size of cell, the substrate can affect the cell adhesion and growth behavior in much more extent. The 3D printed PLA patterns of different stripe widths have different degrees of orientation, and in the range of 0.05–0.3 mm. The smaller the stripe width, the more suitable for hMSCs cell orientation. Cells cultured on smooth glass have a more rounded cell morphology, but a more elongated cell morphology on a 3D printed PLA pattern. Quantitative analysis of the degree of cell orientation was then conducted. The angle between the growth axis of the cell and the standard line is called the positioning angle, and the degree of the positioning angle is used to quantitatively evaluate the degree of “contact guidance” of the cells (Fig. 10B). The smaller the positioning angle, the higher the degree of contact guidance. The direction of the 3D printed PLA stripe pattern is the standard line direction (0°), the orientation angle distribution becomes wider as the stripe width increases. The average orientation angle is close to 0° when the stripe width is 0.05 mm, and the blank control group has a large orientation angle of cells ranging from −90° to 90°. This suggests the cell can grow according to the direction of the PLA stripe, but the cell in the control group is distributed in arbitrary direction. The cell orientation angles of -90° to 90° of different samples were taken as absolute values and the average value can be calculated (Fig. 10C). It also can be seen the average orientation angle of the cells decreases as the width of the stripe decreases. The average orientation angle of the 0.05 mm HNTs-coated PLA pattern is lowest at 2.49°. This is because the cell is limited by the geometric pattern of the substrate during spreading, forcing the pseudopod to grow only along the stripe direction [49]. In our previous work, the patterned HNTs surface can also exhibit a high contact guiding ability for cells. For example, the concentric ring-like HNTs pattern prepared via evaporation-induced self-assembly can guide the growth and orientation of C2C12 myoblast cells perpendicular to the rings [24].

The CCK-8 assay was further used to assess the hMSCs cytotoxicity of the different materials at 1, 3 and 8 days (Fig. 10D). It can be observed that the OD value of hMSCs on all the surfaces gradually increase with the incubation time. The OD value of the hMSCs on PLA patterns of various modification methods are significantly higher than those of the pure PLA pattern after 1 and 3 days incubation. This demonstrates that both HNTs coating and PDA coating can improve the adhesion of cells to the PLA pattern. The 8-day results indicate a lower OD value compared with pure PLA patterns, which is attributed to that coated HNTs may be dropped off from the PLA after a long time immersing in the culture medium. And the dropped HNTs may show certain cytotoxicity. The OD value of the PLA patterns modified by PDA@HNTs coating is maintained at a high level, probably because the PDA encapsulates the HNTs which increase the adhesion of HNTs on PLA which improves biocompatibility [56]. The attachment and proliferation of cells can be affected by many factors, such as surface chemical composition, roughness and hydrophilicity/hydrophobicity. A rough surface with an increased specific surface area can promote the diffusion of liquids, oxygen and biologically active substances for cell proliferation and differentiation [45,57]. In summary, it can be concluded that the improvement of cell adhesion and alignment of PLA pattern after modification by PDA and HNTs is mainly due to the improvement of biological activity and surface roughness of PDA and HNTs.

4. Conclusions

HNTs coated 3D printed PLA pattern with different stripe widths was prepared by immersing the printed PLA structure into PDA and HNTs solution for improving the cell orientation functions. After dopamine polymerization, a layer of PDA@HNTs is coated uniformly on PLA pattern. SEM, POM, and 3D profiler image revealed that a series of 3D printed PLA patterns with different stripes were obtained. FE-SEM, XPS, FTIR, TG, and WCA measurements confirmed that the HNTs coating was bound to the surface of 3D printed PLA with the aid of PDA. The HNTs coating can effectively improve the surface roughness and hydrophilicity of the 3D printed PLA pattern. The 3D printed PLA patterns with different stripes had different ability to induce cell orientation. The smaller the stripe width of the PLA pattern, the more suitable for cell orientation. When the layer height was set to 0.05 mm, the effect of inducing cell orientation was the best. The 3D printed PLA pattern with HNTs coating is more appropriate to adhesion and proliferation of cells. This works provides a general routine for improving the cell affinity of 3D printed PLA structure by HNTs coating, which shows the promising application in cell culture scaffolds, wound healing materials, and biosensors.

Acknowledgments

This work was financially supported by National Natural Science Foundation of China (51473069 and 51502113), Science and Technology Planning Project of Guangdong Province (2014A020217006), Guangdong Special support program (2014TQ01C127), the Pearl River S&T Nova Program of Guangzhou (201610010026).

Appendix A. Supplementary data

Supplementary data to this article can be found online at https://doi.org/10.1016/j.cej.2018.11.145.

References

[1] S.H. Ku, J.S. Lee, C.B. Park, Spatial control of cell adhesion and patterning through mussel-inspired surface modification by polydopamine, Langmuir 26 (2010) 15104–15108.
[2] H.-W. Chien, W.-B. Tsai, Fabrication of tunable micropatterned substrates for cell patterning via microcontact printing of polydopamine with poly(ethylene imine)-grafted copolymers, Acta Biomater. 8 (2012) 3678–3686.
[3] M.M. Stevens, J.H. George, Exploring and engineering the cell surface interface, Science 310 (2005) 1135–1138.
[4] N.M. Alves, I. Pashkuleva, R.L. Reis, J.F. Mano, Controlling cell behavior through the design of polymer surfaces, Small 6 (2010) 2208–2220.
[5] M. Veiseh, B.T. Wickes, D.G. Castner, M. Zhang, Guided cell patterning on gold—silicon dioxide substrates by surface molecular engineering, Biomaterials 25 (2004) 3315–3324.
[6] H.-J. Bai, M.-L. Shao, H.-L. Gou, J.-J. Xu, H.-Y. Chen, Patterned Au/poly(dimethylsiloxane) substrate fabricated by chemical plating coupled with electrochemical etching for cell patterning, Langmuir 25 (2009) 10402–10407.
[7] Y.V. Pan, T.C. McDevitt, T.K. Kim, D. Leach-Scampavia, P.S. Stayton, D.D. Denton, B.D. Ratner, Micro-scale cell patterning on nonfouling plasma polymerized tetraglyme coatings by protein microcontact printing, Plasma Polym. 7 (2002) 171–183.
[8] M. Liu, Z. Huo, T. Liu, Y. Shen, R. He, C. Zhou, Self-assembling halloysite nanotubes into concentric ring patterns in a sphere-on-flat geometry, Langmuir 33 (2017) 3088–3098.
[9] J.-C. Chang, S. Fujita, H. Tonami, K. Kato, H. Iwata, S.-H. Hsu, Cell orientation and regulation of cell-cell communication in human mesenchymal stem cells on different patterns of electrospun fibers, Biomed. Mater. 8 (2013) 055002.
[10] Z. Yi, L. Jian, Z. Haoshen, I. Toshihiro, M. Ryutaro, Effects of the nanoimprint pattern on the performance of a MEMS-based micro direct methanol fuel cell, J.

Micromech. Microeng. 19 (2009) 015003.
[11] D.K. Patel, A.H. Sakhaei, M. Layani, B. Zhang, Q. Ge, S. Magdassi, Highly stretchable and UV curable elastomers for digital light processing based 3D printing, Adv. Mater. 29 (2017) 1606000.
[12] B.C. Gross, J.L. Erkal, S.Y. Lockwood, C. Chen, D.M. Spence, Evaluation of 3D printing and its potential impact on biotechnology and the chemical sciences, Anal. Chem. 86 (2014) 3240–3253.
[13] C.-T. Kao, C.-C. Lin, Y.-W. Chen, C.-H. Yeh, H.-Y. Fang, M.-Y. Shie, Poly(dopamine) coating of 3D printed poly(lactic acid) scaffolds for bone tissue engineering, Mater. Sci. Eng., C 56 (2015) 165–173.
[14] F. Diomede, A. Gugliandolo, P. Cardelli, I. Merciaro, V. Ettorre, T. Traini, R. Bedini, D. Scionti, A. Bramanti, A. Nanci, S. Caputi, A. Fontana, E. Mazzon, O. Trubiani, Three-dimensional printed PLA scaffold and human gingival stem cell-derived extracellular vesicles: a new tool for bone defect repair, Stem Cell Res. Ther. 9 (2018) 104.
[15] B. De la Riva, C. Nowak, E. Sánchez, A. Hernández, M. Schulz-Siegmund, M.K. Pec, A. Delgado, C. Évora, VEGF-controlled release within a bone defect from alginate/chitosan/PLA-H scaffolds, Eur. J. Pharm. Biopharm. 73 (2009) 50–58.
[16] T. Patrício, P. Bártolo, Thermal stability of PCL/PLA blends produced by physical blending process, Procedia Eng. 59 (2013) 292–297.
[17] X. Wang, G. Li, Y. Liu, W. Yu, Q. Sun, Biocompatibility of biological material polylactic acid with stem cells from human exfoliated deciduous teeth, Biomed. Rep. 6 (2017) 519–524.
[18] S.K. Sahoo, A.K. Panda, V. Labhasetwar, Characterization of porous PLGA/PLA microparticles as a scaffold for three dimensional growth of breast cancer cells, Biomacromolecules 6 (2005) 1132–1139.
[19] Y.M. Lvov, D.G. Shchukin, H. Möhwald, R.R. Price, Halloysite clay nanotubes for controlled release of protective agents, ACS Nano 2 (2008) 814–820.
[20] T. Zhu, C. Qian, W. Zheng, R. Bei, S. Liu, Z. Chi, X. Chen, Y. Zhang, J. Xu, Modified halloysite nanotube filled polyimide composites for film capacitors: high dielectric constant, low dielectric loss and excellent heat resistance, RSC Adv. 8 (2018) 10522–10531.
[21] E. Abdullayev, R. Price, D. Shchukin, Y. Lvov, Halloysite tubes as nanocontainers for anticorrosion coating with benzotriazole, ACS Appl. Mater. Interfaces 1 (2009) 1437–1443.
[22] M. Liu, Y. Zhang, C. Zhou, Nanocomposites of halloysite and polylactide, Appl. Clay Sci. 75–76 (2013) 52–59.
[23] R.J. Smith, K.M. Holder, S. Ruiz, W. Hahn, Y. Song, Y.M. Lvov, J.C. Grunlan, Environmentally benign halloysite nanotube multilayer assembly significantly reduces polyurethane flammability, Adv. Funct. Mater. 28 (2017) 1703289.
[24] L. Qin, Y. Zhao, J. Liu, J. Hou, Y. Zhang, J. Wang, J. Zhu, B. Zhang, Y. Lvov, B. Van der Bruggen, Oriented clay nanotube membrane assembled on microporous polymeric substrates, ACS Appl. Mater. Interfaces 8 (2016) 34914–34923.
[25] Y. Liu, W. Tu, M. Chen, L. Ma, B. Yang, Q. Liang, Y. Chen, A mussel-induced method to fabricate reduced graphene oxide/halloysite nanotubes membranes for multifunctional applications in water purification and oil/water separation, Chem. Eng. J. 336 (2018) 263–277.
[26] R. He, M. Liu, Y. Shen, Z. Long, C. Zhou, Large-area assembly of halloysite nanotubes for enhancing the capture of tumor cells, J. Mater. Chem. B 5 (2017) 1712–1723.
[27] G. Lazzara, G. Cavallaro, A. Panchal, R. Fakhrullin, A. Stavitskaya, V. Vinokurov, Y. Lvov, An assembly of organic-inorganic composites using halloysite clay nanotubes, Curr. Opin. Colloid Interface Sci. 35 (2018) 42–50.
[28] R.F. Kamalieva, I.R. Ishmukhametov, S.N. Batasheva, E.V. Rozhina, R.F. Fakhrullin, Uptake of halloysite clay nanotubes by human cells: colourimetric viability tests and microscopy study, Nano-Struct. Nano-Objects 15 (2018) 54–60.
[29] A.V. Stavitskaya, A.A. Novikov, M.S. Kotelev, D.S. Kopitsyn, E.V. Rozhina, I.R. Ishmukhametov, R.F. Fakhrullin, E.V. Ivanov, Y.M. Lvov, V.A. Vinokurov, Fluorescence and cytotoxicity of cadmium sulfide quantum dots stabilized on clay nanotubes, Nanomaterials 8 (2018) 391.
[30] G. Cavallaro, G. Lazzara, S. Konnova, R. Fakhrullin, Y. Lvov, Composite films of natural clay nanotubes with cellulose and chitosan, Green Mater. 2 (2014) 232–242.
[31] Giuseppe, S. Riela, R.F. Fakhrullin, Clay-based drug-delivery systems: what does the future hold? Ther. Del. 8 (2017) 633–646.
[32] R. von Klitzing, D. Stehl, T. Pogrzeba, R. Schomäcker, R. Minullina, A. Panchal, S. Konnova, R. Fakhrullin, J. Koetz, H. Möhwald, Y. Lvov, Halloysites stabilized emulsions for hydroformylation of long chain olefins, Adv. Mater. Interfaces 4 (2017) 1600435.
[33] M.E. Lynge, d.W.R. Van, A. Postma, B. Städler, Polydopamine–a nature-inspired polymer coating for biomedical science, Nanoscale 3 (2011) 4916–4928.
[34] Z. Wang, C. Li, J. Xu, K. Wang, X. Lu, H. Zhang, S. Qu, G. Zhen, F. Ren, Bioadhesive microporous architectures by self-assembling polydopamine microcapsules for biomedical applications, Chem. Mater. 27 (2015) 848–856.
[35] R.S. Hebbar, A.M. Isloor, K. Ananda, A.F. Ismail, Fabrication of polydopamine functionalized halloysite nanotube/polyetherimide membranes for heavy metal removal, J. Mater. Chem. A 4 (2016) 764–774.
[36] S. Ganguly, T.K. Das, S. Mondal, N.C. Das, Synthesis of polydopamine-coated halloysite nanotube-based hydrogel for controlled release of a calcium channel blocker, RSC Adv. 6 (2016) 105350–105362.
[37] S. Cao, P. Xu, Y. Ma, X. Yao, Y. Yao, M. Zong, X. Li, W. Lou, Recent advances in immobilized enzymes on nanocarriers, Chin. J. Catal. 37 (2016) 1814–1823.
[38] X. Wan, Y. Zhan, Z. Long, G. Zeng, Y. He, Core@double-shell structured magnetic halloysite nanotube nano-hybrid as efficient recyclable adsorbent for methylene blue removal, Chem. Eng. J. 330 (2017).
[39] C. Chao, J. Liu, J. Wang, Y. Zhang, B. Zhang, Y. Zhang, X. Xiang, R. Chen, Surface modification of halloysite nanotubes with dopamine for enzyme immobilization, ACS Appl. Mater. Interfaces 5 (2013) 10559–10564.
[40] W.O. Yah, H. Xu, H. Soejima, W. Ma, Y. Lvov, A. Takahara, Biomimetic dopamine derivative for selective polymer modification of halloysite nanotube lumen, J. Am. Chem. Soc. 134 (2012) 12134–12137.
[41] N.F.D. Vecchia, R. Avolio, M. Alfè, M.E. Errico, A. Napolitano, M. D'Ischia, Building-block diversity in polydopamine underpins a multifunctional eumelanin-type platform tunable through a quinone control point, Adv. Funct. Mater. 23 (2013) 1331–1340.
[42] K. Feng, G.-Y. Hung, J. Liu, M. Li, C. Zhou, M. Liu, Fabrication of high performance superhydrophobic coatings by spray-coating of polysiloxane modified halloysite nanotubes, Chem. Eng. J. 331 (2018) 744–754.
[43] W.A. Loesberg, X.F. Walboomers, E.M. Bronkhorst, J.J. van Loon, J.A. Jansen, The effect of combined simulated microgravity and microgrooved surface topography on fibroblasts, Cytoskeleton 64 (2007) 174–185.
[44] V.A. Liu, W.E. Jastromb, S.N. Bhatia, Engineering protein and cell adhesivity using PEO-terminated triblock polymers, J. Biomed. Mater. Res. 60 (2010) 126–134.
[45] H. Liu, W. Li, B. Luo, X. Chen, W. Wen, C. Zhou, Icariin immobilized electrospinning poly(l-lactide) fibrous membranes via polydopamine adhesive coating with enhanced cytocompatibility and osteogenic activity, Mater. Sci. Eng., C 79 (2017) 399–409.
[46] L. Mammen, X. Deng, M. Untch, D. Vijayshankar, P. Papadopoulos, R. Berger, E. Riccardi, F. Leroy, D. Vollmer, Effect of nanoroughness on highly hydrophobic and superhydrophobic coatings, Langmuir 28 (2012) 15005–15014.
[47] P.Y. Wang, H.T. Yu, W.B. Tsai, Modulation of alignment and differentiation of skeletal myoblasts by submicron ridges/grooves surface structure, Biotechnol. Bioeng. 106 (2010) 285–294.
[48] R.-Z. Lin, C.-T. Ho, C.-H. Liu, H.-Y. Chang, Dielectrophoresis based-cell patterning for tissue engineering, Biotechnol. J. 1 (2006) 949–957.
[49] A.I. Teixeira, G.A. Abrams, P.J. Bertics, C.J. Murphy, P.F. Nealey, Epithelial contact guidance on well-defined micro- and nanostructured substrates, J. Cell Sci. 116 (2003) 1881–1892.
[50] N. Li, Q. Zhang, S. Gao, Q. Song, R. Huang, L. Wang, L. Liu, J. Dai, M. Tang, G. Cheng, Three-dimensional graphene foam as a biocompatible and conductive scaffold for neural stem cells, Sci. Rep. 3 (2013) 132.
[51] G. Zeng, Z. Ye, Y. He, X. Yang, J. Ma, H. Shi, Z. Feng, Application of dopamine-modified halloysite nanotubes/PVDF blend membranes for direct dyes removal from wastewater, Chem. Eng. J. 323 (2017) 572–583.
[52] X. Liu, J. Cao, H. Li, J. Li, Q. Jin, K. Ren, J. Ji, Mussel-inspired polydopamine: a biocompatible and ultrastable coating for nanoparticles in vivo, ACS Nano 7 (2013) 9384–9395.
[53] J. Kim, I.S. Kim, T.H. Cho, K.B. Lee, S.J. Hwang, G. Tae, I. Noh, S.H. Lee, Y. Park, K. Sun, Bone regeneration using hyaluronic acid-based hydrogel with bone morphogenic protein-2 and human mesenchymal stem cells, Biomaterials 28 (2007) 1830–1837.
[54] N.S. Hwang, S. Varghese, H.J. Lee, Z. Zhang, Z. Ye, J. Bae, L. Cheng, J. Elisseeff, In vivo commitment and functional tissue regeneration using human embryonic stem cell-derived mesenchymal cells, PNAS 105 (2008) 20641.
[55] E.J. Lee, J.W. Holmes, K.D. Costa, Remodeling of engineered tissue anisotropy in response to altered loading conditions, Ann. Biomed. Eng. 36 (2008) 1322–1334.
[56] C. Luo, Z. Zou, B. Luo, W. Wen, H. Li, M. Liu, C. Zhou, Enhanced mechanical properties and cytocompatibility of electrospun poly(l-lactide) composite fiber membranes assisted by polydopamine-coated halloysite nanotubes, Appl. Surf. Sci. 369 (2016) 82–91.
[57] S. Çakmak, A.S. Çakmak, D.L. Kaplan, M. Gümüşderelioğlu, A silk fibroin and peptide amphiphile-based co-culture model for osteochondral tissue engineering, Macromol. Biosci. 16 (2016) 1212–1226.